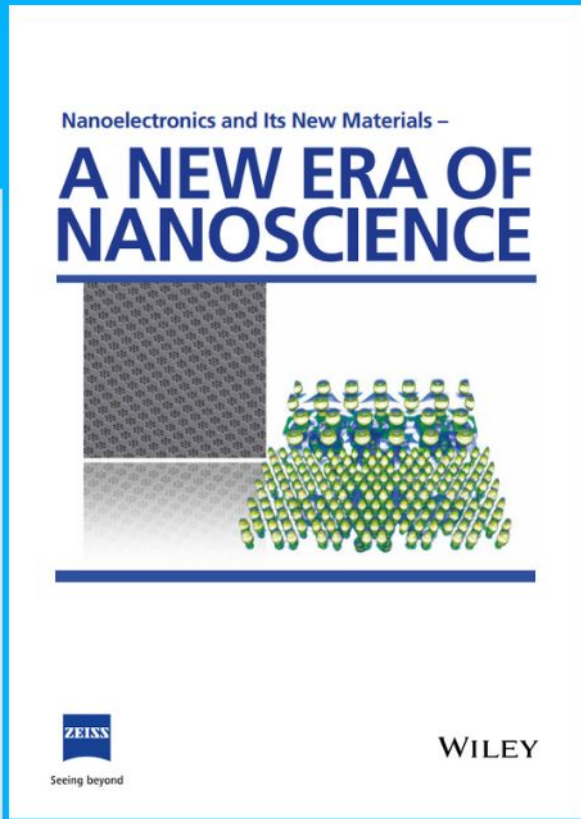




Nanoelectronics and Its New Materials – A NEW ERA OF NANOSCIENCE



Discover the recent advances in electronics research and fundamental nanoscience.

Nanotechnology has become the driving force behind breakthroughs in engineering, materials science, physics, chemistry, and biological sciences. In this compendium, we delve into a wide range of novel applications that highlight recent advances in electronics research and fundamental nanoscience. From surface analysis and defect detection to tailored optical functionality and transparent nanowire electrodes, this eBook covers key topics that will revolutionize the future of electronics.

To get your hands on this valuable resource and unleash the power of nanotechnology, simply download the eBook now. Stay ahead of the curve and embrace the future of electronics with nanoscience as your guide.



Seeing beyond

WILEY

Launching a Drop via Interplay of Buoyancy and Stick-Jump Dissolution

Binglin Zeng,* Haichang Yang, Ben Bin Xu, Detlef Lohse,* and Xuehua Zhang*

According to Archimedes' principle, a submerged object with a density lower than that of aqueous acid solution is more buoyant than a smaller one. In this work, a remarkable phenomenon is reported wherein a dissolving drop on a substrate rises in the water only after it has diminished to a much smaller size, though the buoyancy is smaller. The drop consisting of a polymer solution reacts with the acid in the surrounding, yielding a water-soluble product. During drop dissolution, water-rich microdroplets form within the drop, merging with the external aqueous phase along the drop-substrate boundary. Two key elements determine the drop rise dynamics. The first is the stick-jump behavior during drop dissolution. The second is that buoyancy exerts a strong enough force on the drop at an Archimedean number greater than 1, while the stick-jump behavior is ongoing. The time of the drop rise is controlled by the initial size and the reaction rate of the drop. This novel mechanism for programmable drop rise may be beneficial for many future applications, such as microfluidics, microrobotics, and device engineering where the spontaneous drop detachment may be utilized to trigger a cascade of events in a dense medium.

reduce the adhesion force between the drop and the surface. For instance, on superhydrophobic or omniphobic surfaces, drops are partially supported by an air cushion.^[9] The release of surface energy from drop coalescence can result in the drop detaching from the surface and jumping into the air.^[10] On slippery liquid-like surfaces, the lubricated drops can roll off with minimal hysteresis in their contact angles.^[11–14] In this paper, we want to present a new phenomenon which may contribute to new concepts that can be leveraged to develop effective strategies for controlling drop mobility in a dense medium.

The adhesion force along the drop boundary can be reduced through the self-lubricating effect of a complex multicomponent drop on a smooth surface. In particular, the evaporation or dissolution of a drop component may result in liquid-liquid phase separation and the formation of microdroplets of an immiscible fluid within the drop.^[15–17] As

an example, during the evaporation of a ternary drop consisting of water, ethanol, and oil, microdroplets of oil form at the drop rim due to the preferential evaporation of ethanol. These microdroplets accumulate to a continuous circular self-lubricating ring.^[16,17] The self-lubrication can be highly effective in counteracting the pinning effect, even from the evaporation of a drop containing nanoparticles.^[17]

Another boundary condition to achieve drop mobility is the activation, which can be powered by surface tension gradients.^[18–20]

1. Introduction

Spontaneous drop departure from a surface is a crucial process in both natural and technological systems. The process plays a significant role in collecting water from air,^[1,2] harvesting energy from rainfall,^[3,4] and creating self-cleaning and anti-icing surfaces.^[5] Recently, the primary strategy to enhance drop mobility is to exploit various bio-inspired surfaces that are decorated with sophisticated micro- and nanotextures.^[6–8] The goal is to


B. Zeng, H. Yang, X. Zhang
Department of Chemical and Materials Engineering
University of Alberta
Edmonton T6G 1H9, Canada
E-mail: binglin@ualberta.ca; xuehua.zhang@ualberta.ca

H. Yang
School of Chemical Engineering and Technology
China University of Mining and Technology
Xuzhou 221116, China

B. B. Xu
Mechanical and Construction Engineering
Faculty of Engineering and Environment
Northumbria University
Newcastle Upon Tyne NE1 8ST, UK

D. Lohse, X. Zhang
Physics of Fluids Group
Max Planck Center for Complex Fluid Dynamics
University of Twente
Enschede 7500 AE, The Netherlands
E-mail: d.lohse@utwente.nl

D. Lohse
Max Planck Institute for Dynamics and Self-Organization
37077 Göttingen, Germany

 The ORCID identification number(s) for the author(s) of this article can be found under <https://doi.org/10.1002/smll.202303177>

© 2023 The Authors. Small published by Wiley-VCH GmbH. This is an open access article under the terms of the Creative Commons Attribution License, which permits use, distribution and reproduction in any medium, provided the original work is properly cited.

DOI: 10.1002/smll.202303177

Such temporal and spatial gradients can be created through various physical or chemical processes, including inhomogeneous mixing, solubilization or miscellization of surfactants adsorbed on the drop surface, and chemical reactions of the drop.^[21–23] The resulting surface tension gradient can then reconfigure the drop morphology and induce complex internal, interfacial, and external flows.^[24,25] The induced external flow may, in turn, drive the motion of the drop.^[26,27] For example, the autonomous movement of a drop microswimmer can be propelled by a force generated from a concentration gradient that arises from surfactant miscellization.^[18,28] Microdrops confined in quasi-2D spaces can be propelled by a force generated from the concentration gradient formed through liquid–liquid phase separation.^[29,30] Furthermore, chemical reactions that take place in or on the drop surface may produce a chemical concentration gradient of a reactant or product, which can be used to drive the drops.^[31,32] However, it is unclear how a reaction can initiate the programmable drop detachment without the involvement of a surfactant-like compound.

In this work, we have discovered a fascinating phenomenon in which a dissolving drop submerged in an aqueous solution, once it reaches a certain reduced size, rises suddenly from the surface. The spontaneous rise of the drop is regulated by two key elements: the stick-jump behavior of the drop in the presence of internal microdroplets and an Archimedes number greater than one, which indicates that the buoyant force on the dissolving drop is stronger than the viscosity of the surrounding liquid medium. In contrast to aforementioned rising mechanisms, we propose for the first time that the mechanism for a rising droplet is attributed to both droplet dissolution and buoyancy. Our finding offers new opportunities for controlling drop movement in a range of applications, such as microrobotics, device engineering, and microfluidics, where the spontaneous detachment of a submerged sessile drop could be utilized to initiate a series of events.

2. Results and Discussion

2.1. Observation of the Launch of the Drop

Figure 1a shows the dissolution of a drop consisted of polystyrene (PS) and N,N-dimethylcyclohexylamine (DMCHA) on the substrate immersed in the acid solution. The process is divided into two phases. During phase I over a period of thousands of seconds, the base diameter of the drop L steadily shrinks while maintaining a constant contact angle of $\approx 70^\circ$. The drop dissolution can be attributed to the water-soluble product resulting from the chemical reaction occurring on the surface of the drop. During phase II over a period of less than 200 s, the drop elongates vertically and subsequently detaches from the surface, ascending rapidly and accelerating to a constant velocity $v_s = 2 \text{ mm s}^{-1}$ in just one second, as captured in Movie S1, Supporting Information. The drop then maintains the constant velocity as it continues to rise.

Figure 1b shows the dissolution process of three drops of varying initial volumes, ranging from 0.2 to 3.1 mm^3 . The acid concentration in the solution is 0.2 wt%. In phase I, at 800 and 3000 s, respectively, the smallest drop and then the two larger drops become cloudy as a result of the formation of microdroplets within the drop (see Movie S2, Supporting Information). The two larger

drops detach and rise in phase II, but the smallest drop stays on the substrate until the completion of drop dissolution (see Movie S3, Supporting Information). Similar drop rise phenomena are also observed as the concentration of the acid is changed from 0.2 to 0.5 wt% as illustrated in **Figure 1c**. For all rising drops, along with their three-phase contact lines recede, a liquid bridge forms between the drop and substrate. As the liquid bridge becomes thinner, the host drop eventually detaches as evident in the **Figure 1c**–**d**.

The relationship between the drop rise event, the initial drop volume V_0 , and the concentration of the acid c_a is depicted in the phase diagram in **Figure 1d**. The drop rise can occur for various initial volumes at a given acid concentration. For example, drops with initial volumes ranging from 0.5 to 5.5 mm^3 can rise at an acid concentration of 0.2 wt%. Starting with an initial drop volume of $\approx 1.0 \text{ mm}^3$, the drop rises in a solution with an acid concentration ranging from 0.2 to 0.3 wt%, but does not rise at a concentration of 0.4 and 0.5 wt%. As the acid concentration increases from 0.2 to 0.5 wt%, the minimum initial volume required for the drop to rise also increases from 0.5 to 3.0 mm^3 . This indicates that a larger drop can rise at a wider range of acid concentrations.

The phase diagram in **Figure 1e** shows the relationship between the volume of the detached drop V_s and the initial drop volume V_0 for all rising drops. V_s is smaller for the drop with a smaller V_0 . The data reveals a linear relation between V_s and V_0 , $V_s \propto V_0$.

2.2. Two Requirements for the Drop Rise

2.2.1. Stick-Jump Behavior of Dissolving Drops

In phase II, prior to the drop rise, three instances of stick-jump transitions can be clearly identified in the drop shape as shown in **Figure 2a–c**: the contact angle of the drop from 85° to 92° at $t = t_1 + 41.1 \text{ s}$, from 102° to 116° at $t = t_1 + 91.7 \text{ s}$, and from 120° to 152° at $t = t_1 + 116.1 \text{ s}$ (Movie S4, Supporting Information). Here t_1 represents the starting time at which the contact angle of the host drop begins to increase. Simultaneously, the height of the drop H jumps three times from 0.14 to 0.18 mm, while the contact diameter L decreases three times from 0.32 to 0.09 mm. This stick-jump behavior occurs for the drop already partly dissolved to a smaller size. The reason is that the increase in the drop height is significant for the drop with a small volume at the moment of the contraction of the three-phase boundary along the substrate.^[33]

In contrast, for the non-rising drop with small V_0 shown in **Figure 2d,e**, the maximal height of the drop reaches $\approx 0.07 \text{ mm}$, and then decreases as L decreases from 0.35 to 0.1 mm. The drop maintains contact with the substrate at all times while the contact angle increases and then abruptly decreases from $\approx 135^\circ$ to $\approx 115^\circ$. Such transient jump mode with a high contact angle was observed for all non-rising drops, indicating the stick-jump behavior also occurs for the non-rising drops.

2.2.2. Archimedes Number of Rising Drops

We introduce the Archimedes number (Ar)^[34] as the central parameter that determines the drop rise behavior (**Figure 2f**).

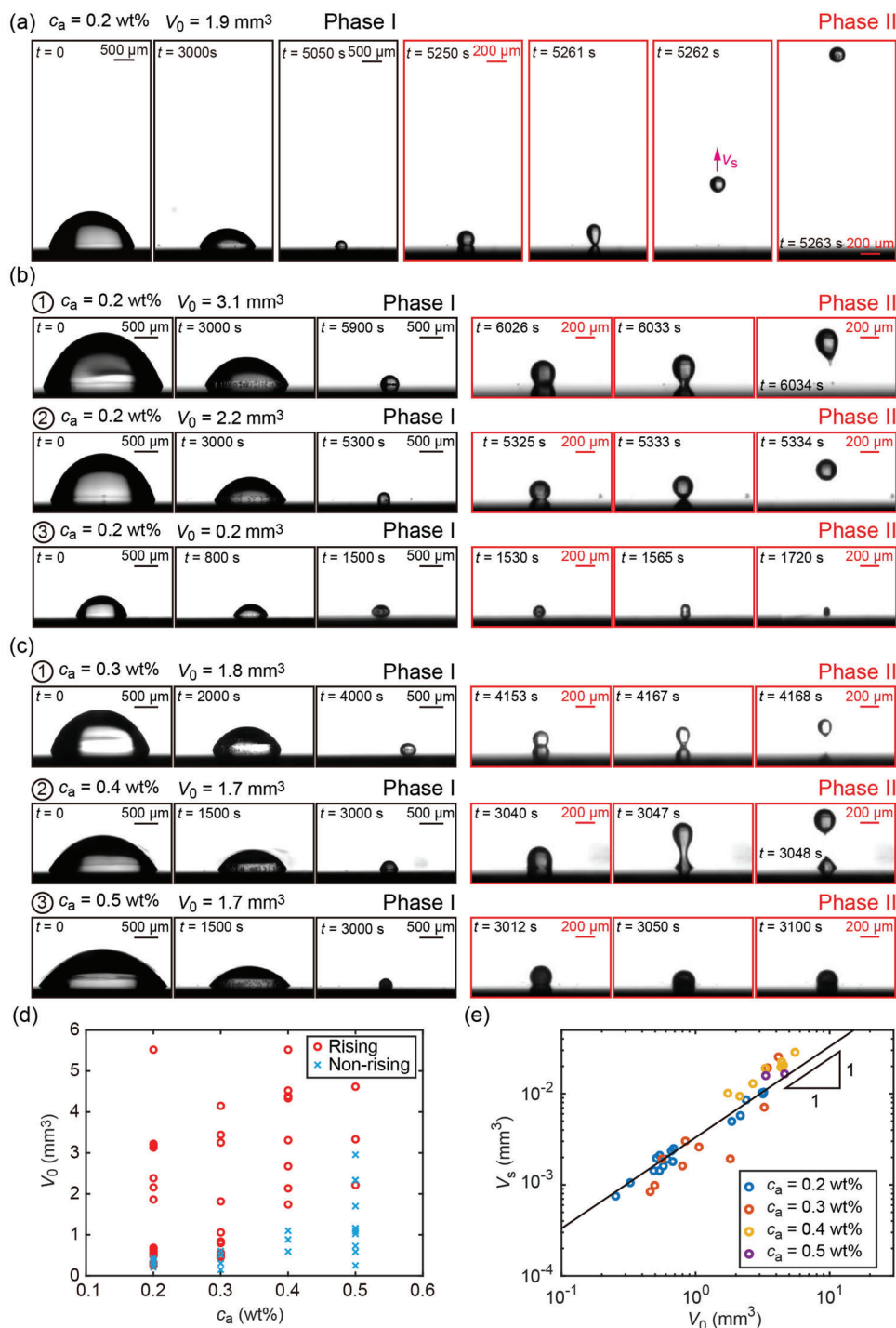


Figure 1. a) Successive snapshots of a dissolving drop that detaches and rises in the aqueous solution. The initial concentration $c_{PS,0}$ of the polymer in the drop is 0.01 wt%. The concentration c_a of formic acid in the aqueous phase is 0.2 wt%. b) Snapshots of the drop submerged in the acid solution of varying initial drop volume V_0 of 0.2, 2.2, and 3.1 mm³. (Black box: Phase I; Red box: Phase 2) c) Snapshots of the drops in the acid solution at the concentration c_a of 0.3, 0.4, and 0.5 wt%. (Black box: Phase I; Red box: Phase 2) d) Phase diagram for drop rise events in an acid aqueous solution with dissolved polymer. As listed in Table 1, the concentration of the acid (c_a) varies from 0.2 wt% to 0.5 wt%, and the initial drop volume ranges from 0.1 mm³ to ≈ 5.5 mm³, with the initial concentration of polymer in the drop $c_{PS,0}$ at 0.01 wt%. e) The volume of the drop V_s upon detachment is a function of its initial volume V_0 , following the linear relation $V_s \propto V_0$.

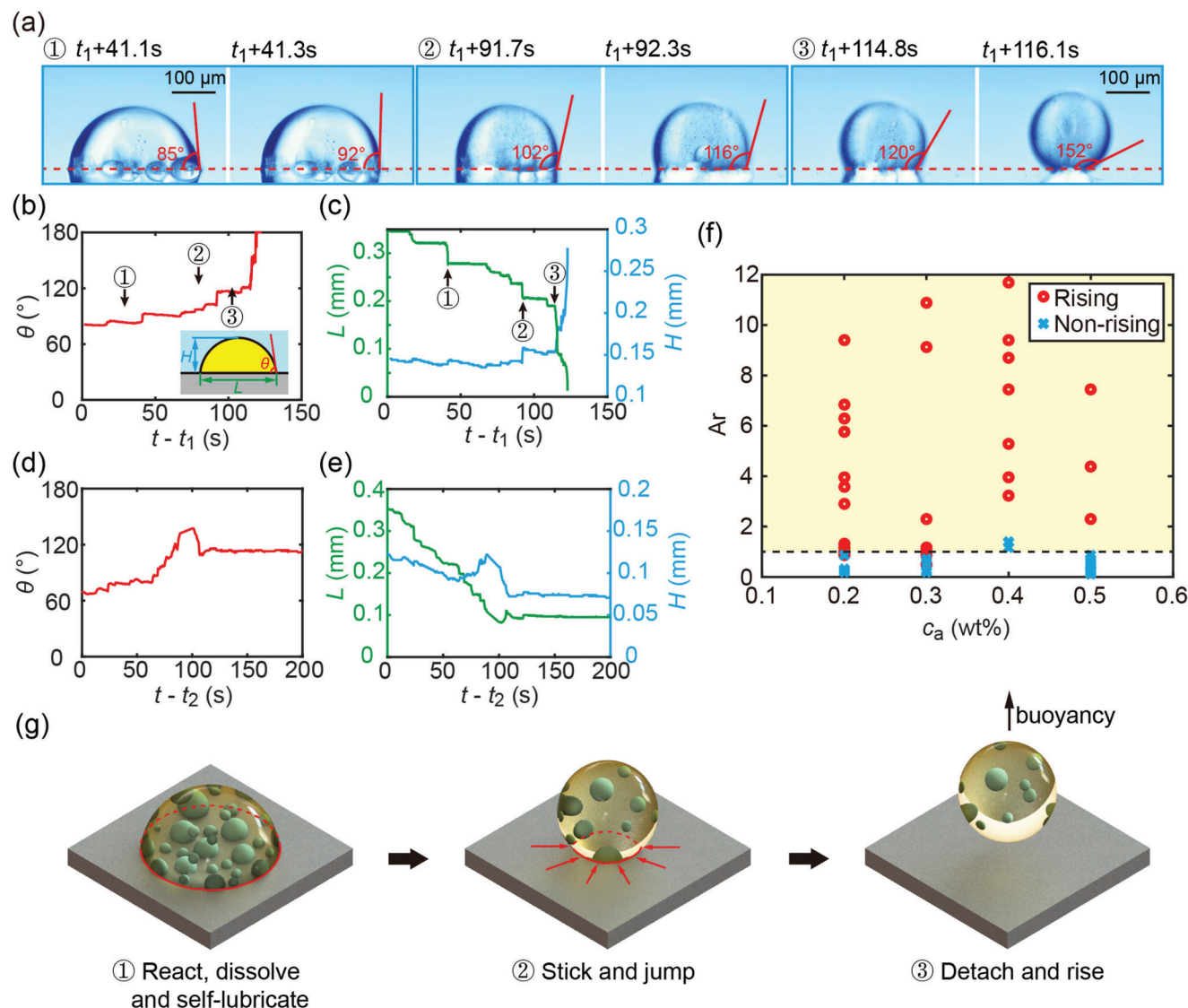


Figure 2. a) Snapshots of a dissolving drop in the aqueous solution in phase II. The contact angle of the drop changes during dissolution, exhibiting a stick-jump behavior. The initial concentration of polymer inside the drop c_{ps} is 0.01 wt%, and the acid concentration in the external solution c_a is 0.2 wt%. b, c) Temporal evolution of contact angle θ , height H , and the base diameter L of the drop. The stick-jump behavior is reflected by the increase in θ and H , prior to the drop detachment. d, e) Temporal evolution of θ , H , and L of a non-rising drop with a small V_0 . f) Ar numbers for all cases in Figure 1d. The rising drops satisfy the condition of $Ar > 1$. g) Schematic the process of detachment and rise of a drop. Red circle: the boundary of the drop and the substrate. ① Dissolution of the host drop and nucleation of internal microdroplets that lubricate the boundary of the host drop; ② Stick-jump behavior of the host drop, depinning as internal microdroplets merge with the surrounding aqueous phase; ③ Increase in θ , and detachment and rise of the drop under buoyancy.

Representing the ratio of gravity and the viscous force, the Ar number is calculated from the radius of the drop

$$Ar = \frac{gR_r^3 \Delta\rho}{\rho_w \nu^2} \quad (1)$$

where g is the gravitational acceleration (9.8 m s^{-2}); R_r refers to either the radius of the host drop immediately prior to detachment for a rising drop, or to the radius of the host drop at its maximum contact angle after exhibiting stick-jump behavior for a non-rising drop; ρ_w is the density of water (1000 kg m^{-3}), and ν , the kinematic viscosity of the aqueous solution at room tem-

perature ($\approx 10^{-6} \text{ m}^2 \text{ s}^{-1}$). The density difference between the drop liquid and water $\Delta\rho$ ($\rho_w - \rho_{DMCHA}$) is 151 kg m^{-3} , where ρ_{DMCHA} is the density of DMCHA. Considering the narrow range of regulation for acid concentration from 0.2 to 0.5 wt%, the changes in density and viscosity of the aqueous formic acid can be neglected.

The Ar numbers of 60 drops are obtained from the experiments and are illustrated in Figure 2f. The Ar number is > 1 for all rising drops, indicating that the buoyancy can overwhelm the viscous force and drive the drop to detach and rise. The Ar number is ≤ 1 for all non-rising drops. But note that the buoyancy of the drop is initially larger due to the drop's larger volume and thus height, and decreases as the drop dissolves. Thus, buoyancy

alone is insufficient to explain why only partly dissolved drops detach from the substrate, not the larger initial drops, though their Archimedes number is larger than 1.

2.2.3. Interplay of Buoyancy and Stick-Jump Dissolution

We propose that to initiate the detachment and ascent of the drop, two conditions must be fulfilled: first, the Ar number must exceed one, so that buoyancy can overcome viscosity and facilitate drop detachment as discussed, as second, internal water microdroplets must induce the stick-jump dissolution behavior. The process is illustrated in Figure 2g.

The sessile microdroplets forming within the host drop are essential to the contraction of the drop boundary. The coalescence of internal sessile microdroplets and the surrounding aqueous environment lubricates the boundary of the drop. As the contact area decreases and the contact angle increases beyond 90°, the pinning effect of the drop to the surface is significantly reduced. The pinning force is proportional to γP , where γ is the interfacial tension between the host drop and surrounding, and P is the perimeter of the three-phase contact line. Consequently, the buoyancy force surpasses the pinning force, leading to detachment of the drop from the substrate.

To verify the reduced adhesion caused by lubricating merging sessile microdroplets, a host drop was placed upside-down to dissolve in the acid solution of 0.2 wt%. With V_0 of 1.33 mm³, the drop would rise if placed upright. At the end, the upside-down drop could still detach from the substrate, as demonstrated in Movie S5, Supporting Information.

Self-lubrication by water microdroplets is insensitive to the chemical properties of the substrate. The drops can be launched from various substrates, including bare glass, (3-aminopropyl) triethoxysilane coated and octadecyltrichlorosilane coated substrates. The snapshots of rising drops on those substrates are provided in Supporting Information (Movies S6–S8, Supporting Information).

2.3. Dynamics of Internal Water Microdroplets

To gain further insight into the microdroplet formation within the dissolving drop, we captured the confocal images in Figure 3a to show a host drop with a diameter L_0 of 600 μm dyed red and a surrounding solution dyed green. The images show that the microdroplets within the dissolving drop are dark, due to absence of the dye dissolved in the aqueous phase. These microdroplets were not created through emulsification of the external aqueous solution, but rather, through a phase separation process within the drop. Furthermore, the microdroplets are water-rich, and soluble in the aqueous solution as seen in Movie S9, Supporting Information.

The growth of water microdroplets within the dissolving drops are largely dictated by diffusion. As shown in Figures 3b–f for drops of different sizes, the nucleation of microdroplets was observed after a few hundreds of seconds during drop dissolution (see Movies S10 and S11, Supporting Information). We did not observe any patterns or preferred locations for the micro water droplets, indicating random location for formation of water microdroplets. For all host drops with V_0 between 1 and 7

mm³, their nucleation time t_n lies between 200 and 2000 s. In a diffusion-dominated process^[35,36]

$$t_{\text{diff}} \approx V_0^{2/3} / (\pi D) \approx 10^2 \text{ to } 10^3 \text{ s} \quad (2)$$

where $D \approx 10^{-9} \text{ m}^2 \text{ s}^{-1}$ is the mass diffusivity of water in the host drop. The timescale of mass diffusion in drops of these volumes is in agreement with the measured timescale in Figure 3f.

Figure 3g illustrate the base radius R_w for five representative microdroplets, showing that the R_w experienced a rapid growth in the initial 1000 s, followed by a gradual increase. In the initial stage, the radius growth rate of the microdroplets reaches 0.038 $\mu\text{m s}^{-1}$, and then gradually decreases to 0.004 $\mu\text{m s}^{-1}$ over the course of 1000 s before stabilizing until the drop rise (Figure S2a, Supporting Information). Assuming a diffusion-limited growth,^[37] the temporal evolution of water oversaturation from the difference between the concentration of the water in the host drop $c_{\infty, w}$ and the concentration of water in the boundary layer of microdroplets $c_{s, w}$, can be derived using the theoretical model. The oversaturation of water available for microdroplet formation decreases as the drop dissolution progresses, likely due to the depletion of water from microdroplet growth. The concentration difference of water $c_{\infty, w} - c_{s, w}$ at the interface of the water microdroplet is a function of time t , as calculated from the data in Figure 3g using the mass diffusion equation.^[37] The derivative of the radius with respect to time (dR_w/dt) of five labelled microdroplets is provided in Supporting Information.

As the base area of the host drop decreases (as seen in Figure 3d,i), the aggregate base area of all the immersed sessile microdroplets increases over time. Figure 3j illustrates how the ratio $A_{\text{microdroplets}}/A_{\text{host}}$ steadily increases with time. At ≈ 4800 s, the aggregate coverage of microdroplets on the surface experiences a sudden spike, leading to a peak of the ratio $A_{\text{microdroplets}}/A_{\text{host}}$. This, in turn, reduces the pinning of the drop and the dissolving drop breaks off from the substrate and ascends, as seen in Movie S12, Supporting information. Some tiny water droplets are suspended above the surface (Figure 2a-Ⓞ). But they do not show clear influence on the pinning effect of the host drop. As observed in Movie S4, Supporting Information, there is internal fluid motion within the host drop prior to the rise, carrying them away from the surface.

The formation of internal microdroplets within the host drop may bear a resemblance to liquid–liquid phase separation in multicomponent drops.^[16,25,38] Typically, the preferential dissolution of a drop component leads to the composition change in the drop and a reduced solubility of another component in the drop. Encapsulated microdroplets form from liquid–liquid phase separation in response to the reduced miscibility of the drop components. The oversaturation of water in the drop may be due to the increases in the polymer concentration in the drop, leading to the nucleation and growth of water-rich microdroplets.

The polymer dissolved in the drop is insoluble in the surrounding aqueous solution and remains in the drop.^[39] Assuming that all polymer mass remains trapped inside the drop, the concentration of polymer at the drop detachment volume V_s can be estimated from $m_{\text{PS}} = c_{\text{PS},0} V_0 = c_{\text{PS},s} V_s$, implying

$$c_{\text{PS},s} = c_{\text{PS},0} V_0 / V_s \quad (3)$$

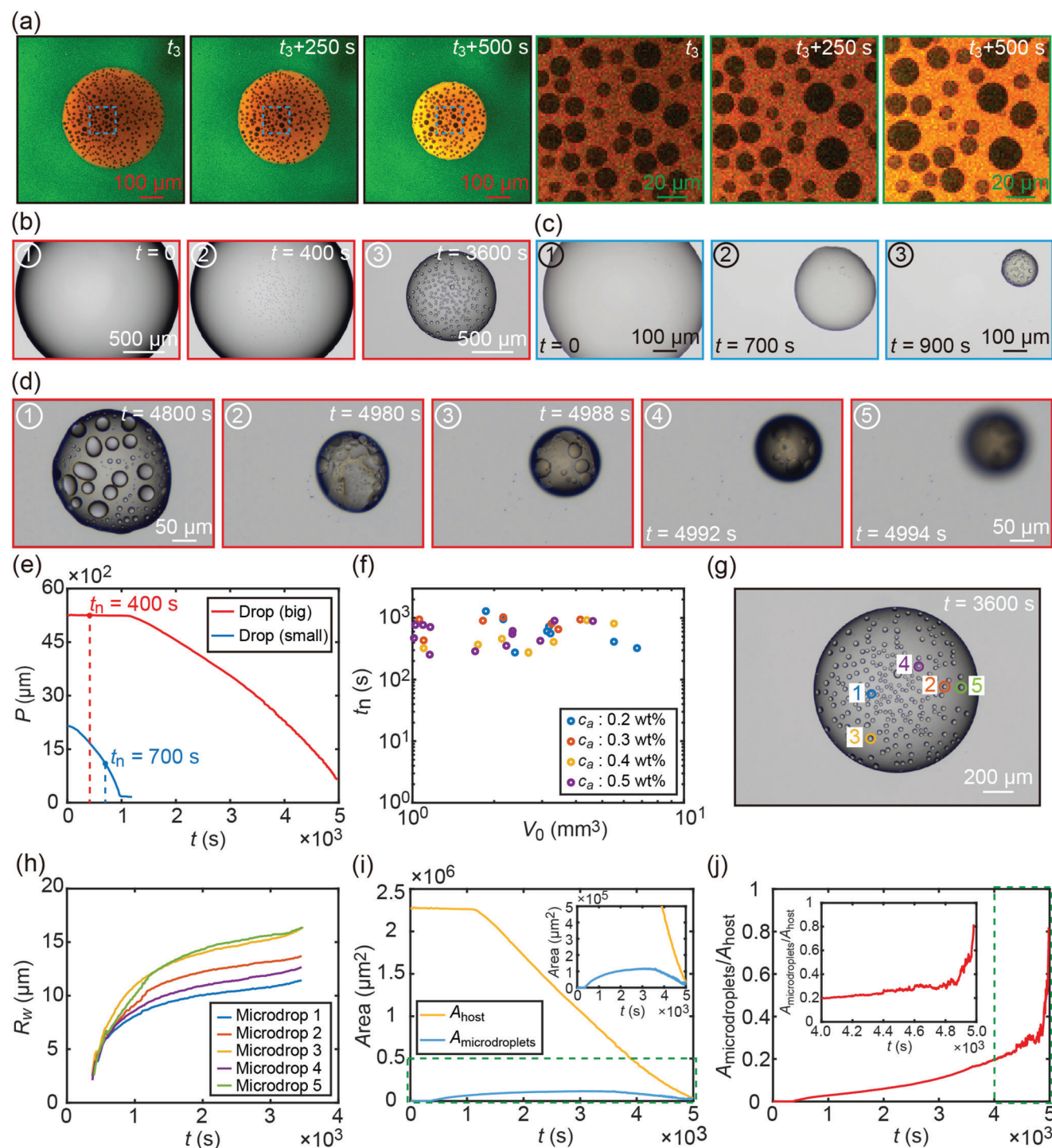


Figure 3. Growth dynamics of internal microdroplets. a) Confocal images depicting the nucleation and growth of water microdroplets inside a host drop with the zoom-in images in the blue box. b,c) Bright-field images of internal microdroplets nucleating and growing within host drops. The initial diameters L_0 of the big drop and small drop are 1.70 (b) and 0.68 mm (c), respectively. d) Zoom-in snapshots of water microdroplets that grow and coalesce within the host drop (big) prior to the detachment. e) Plot of perimeter P of the three phase contact line as a function of time of the two drops shown in (b) and (c). The internal microdroplets appear at the time labeled by the dotted lines. f) The nucleation time t_n of water microdroplets within the host drop as a function of V_0 . c_a is the concentration of the acid in the surrounding solution. g) Five representative microdroplets inside a host drop. h) Temporal evolution of the base radius R_w of the five microdroplets in (g). i) Temporal evolution of the base area of the host drop and the total base area of the sessile water microdroplets within the drop. The inset displays the zoomed-in data labeled by the green dashed line box. j) The ratio of the base area of the host drop to the total area of the water microdroplets. The inset displays zoomed-in data labeled by the green dashed line box. The initial concentration $c_{p,0}$ of the polymer in the drop is 0.01 wt%, and the acid concentration c_a in the solution is 0.2 wt%.

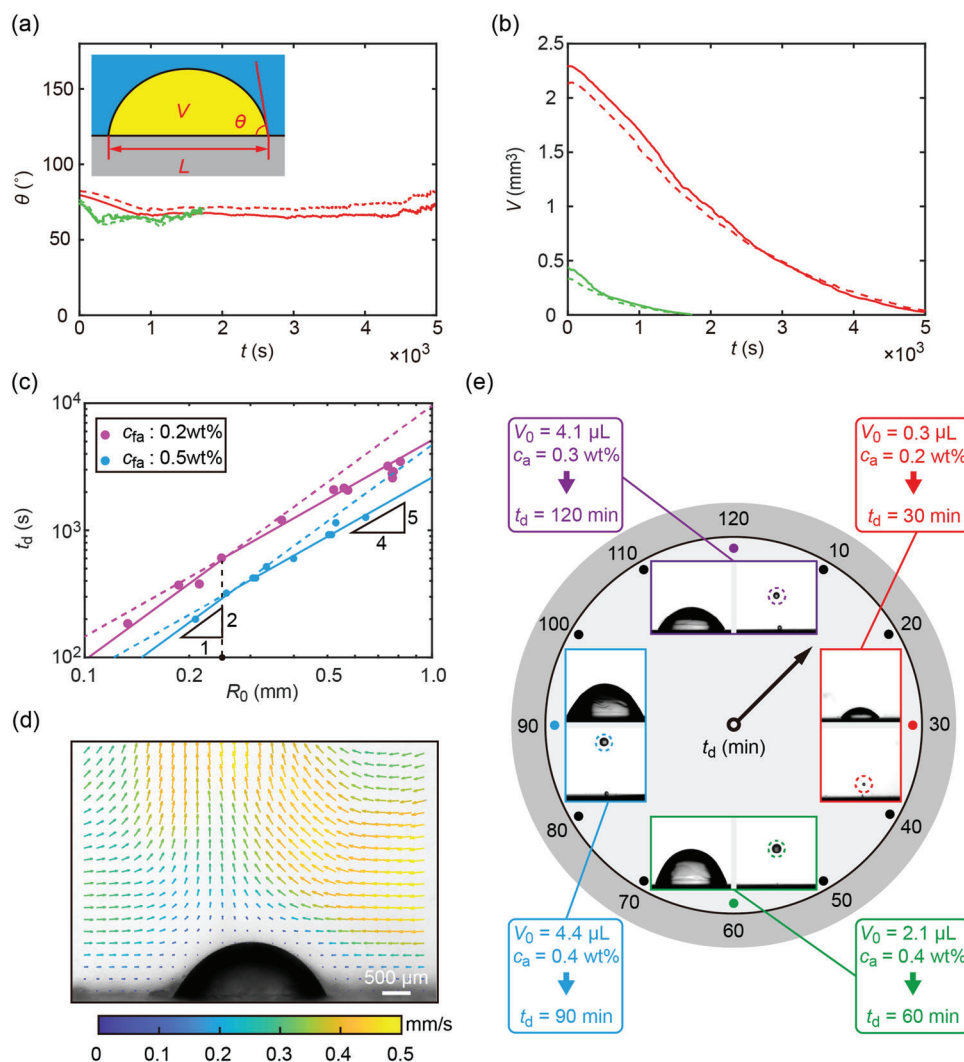


Figure 4. a,b) Temporal evolution of the contact angles θ and volumes V of two drops in Phase I dissolution. The initial drop volumes are roughly 2.2 (red) and 0.5 mm³ (green). Solid and dashed curves come from repeated experiments with nearly the same initial drop volume. The initial polymer concentration $c_{PS,0}$ is 0.01 wt% in the drop, and the acid concentration c_a is 0.2 wt%. c) Dissolution time t_d of the drop as a function of its initial radius R_0 . The scaling laws of $t_d \approx R_0^2$ and $t_d \approx R_0^{5/4}$ indicate that the drop dissolution is dominated by diffusion and by natural convection, respectively. d) Velocity field surrounding a dissolving drop at $t = 150$ s. e) Sketch of setting time for launching the drop.

Here, $c_{PS,0}$ is the initial concentration of the polymer in the host drop and $c_{PS,s}$ the concentration of the polymer in the rising drop of volume V_s . For all rising drops shown in Figure 1d, $c_{PS,s}$ is approximately the same at the drop detachment, reaching up to ≈ 4 wt%. It is possible to achieve this polymer concentration by reducing the initial concentration of the polymer while increasing the initial size of the drop. However, the initial size of the drop must not be overly large, or else the drop floats immediately due to the large buoyancy prior to dissolution. The viscosity ratio between the drop and the surrounding medium might also have some impact on drop detachment. However, it is to determine the viscosity ratio, as the drop dissolution leads to highly heterogeneous spatial distribution of multiple components in the drop, including nucleation of water microdroplets.

2.4. Set Time for Launching the Drop

The duration from the drop deposition to the drop rise is determined by the dynamics of the drop dissolution. Figure 4a,b illustrates a small and a large drop during phase I of the dissolution process.

Varying the initial drop radius R_0 from 150 to 800 μ m at two acid concentrations, the dissolution time t_d follows two scaling laws shown in Figure 4c. For $R_0 \gtrsim 250$ μ m, t_d follows the scaling law $t_d \approx R_0^{5/4}$, for convective dissolution.^[40] For $R_0 \lesssim 250$ μ m, t_d follows the scaling law $t_d \approx R_0^2$, for diffusive dissolution. The convective flow is confirmed by the flow visualization in Figure 4d, obtained from micro-particle image velocimetry (μ PIV) for a drop of $R = 1.35$ mm. An upward flow is seen above the drop apex with the velocities ranging from 0.1 to 0.4 mm s⁻¹. Convection is

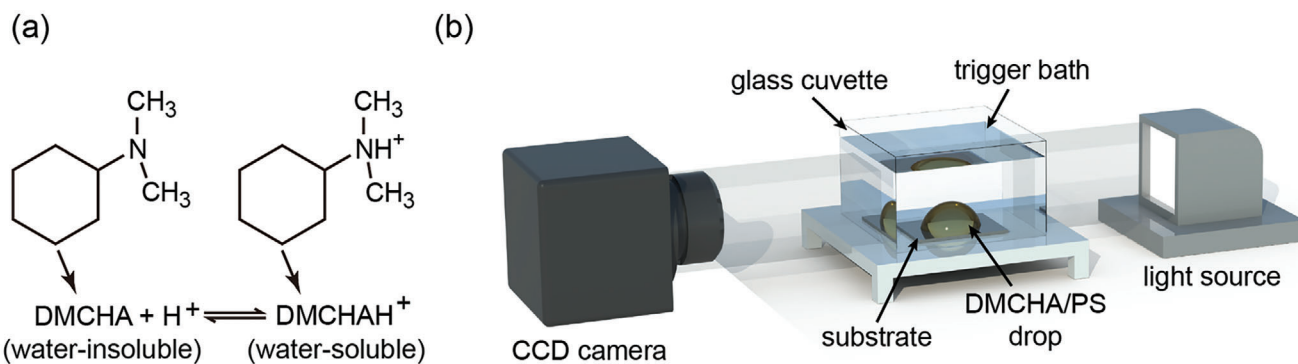


Figure 5. a) Molecular structure of the drop liquid DMCHA and the reaction equation at the drop surface. b) Schematic of the optical system for observation of drop rise.

triggered by the density difference between a lighter, water-soluble product from the reaction at the drop surface and the denser aqueous solution in which the drop is submerged.^[25]

The onset of the natural convection during drop dissolution can be quantified by the Ar number,^[25] as defined in Equation (1), which can be restated as

$$Ar = \frac{gR^3(1 - \cos \theta)^3 \Delta \rho}{\rho_w \nu^2} \quad (4)$$

Considering a drop with a contact angle $\theta \approx 70^\circ$, at Ar of ≈ 1 , R is $\approx 240 \mu\text{m}$, indeed close to transition of R from convective to diffusive dissolution. The transition from convection-driven to diffusion-driven dissolution of the reacting drop is comparable to that of a dissolving pure liquid drop with a density lower than the surrounding fluid.^[40]

The well-controlled dissolution behavior in the long period of phase I enables the control of the time for the drop to rise. A clock of the drop rise shown in Figure 4e is achieved by adjusting the initial drop size according to the relation between t_d versus R_0 . For a given initial size, the acid concentration can be used to tune the time when the drop rises toward shorter times. After the deposition, the time for the drop to detach is at 30, 60, 90, and 120 min. The possibility of setting the clock for the drop rise may be applied to create a gate effect that may initiate a cascade of events in the immersed liquid.

3. Conclusion

Our study has uncovered a new mechanism behind the fascinating phenomenon of spontaneous rise of a submerged drop from a surface. The launch of the dissolving drop is attributed to both buoyancy and the stick-jump behavior of drop boundary during dissolution. Nucleation and growth of internal sessile microdroplets within the host drop weaken the pinning effect at the drop boundary. When the Archimedes number exceeds 1, the buoyancy becomes strong enough to lift the drop. The time for the drop detachment is determined by the initial drop size and the reaction rate of the drop with the surrounding environment.

This spontaneous departure of the drop may have implications for various applications, such as cleaning, decontamination, and separation of oily drops from submerged surfaces. Furthermore, the onset of the directional motion of the drop may be

programmed to trigger a series of events in dense media for microfluidics, microrobotics, and device engineering. Our ongoing work is to develop a gating device that can be switched on and off by the jumping droplet. Another potential application of the rising droplets phenomenon may be to concentrate analytes for sensitive detection. This process involves using droplet dissolution to concentrate the analytes and triggering the rising of the droplets in the final stage for automatic collection.

4. Experimental Section

Chemicals: The acidic aqueous solution was prepared by mixing formic acid (Sigma-Aldrich, America) and water to the concentration of formic acid c_a of 0.2–0.5 wt%. Water used in the experiments was purified from a Milli-Q unit (18.2 M Ω Mill-Q). The drops consisted of PS dissolved in DMCHA. To prepare the PS in DMCHA solution, the polymer particles (molecular weight 35000, Sigma-Aldrich, America) were dissolved into DMCHA (Sigma-Aldrich, America) at the concentration of 0.01 wt%. The molecular structure of DMCHA and the reaction equation with the acid are as shown in Figure 5a. On the drop surface, DMCHA reacted with H⁺ in the external aqueous solution, producing DMCHAH⁺ that is water-soluble.^[38,41]

A silicon slab was used as the substrate for drop dissolution. The substrate was first cleaned in the piranha solution consisting of 70% H₂SO₄–30% H₂O₂ for 30 min, and then cleaned in water for three times with each time for 5 min. (Caution: the piranha solution is highly caustic.) After that, the substrate was dried by a stream of air.

Composition, Size, and Dissolution of Drops: Figure 5b shows the schematic diagram of the experimental setup for visualization of a dissolving drop. The substrate was placed in a rectangular quartz cuvette filled with the aqueous solution of formic acid at a given concentration.

Table 1. Experimental parameters for studying the influence of the initial drop volume V_0 and formic acid concentration c_a on drop dynamics. The initial polymer concentration in the drop c_{PS} is fixed at 0.01 wt%.

c_a [wt%]	V_0 [mm ³]												
0.2	0.20	0.25	0.30	0.33	0.36	0.39	0.44	0.49	0.51	0.54	0.58	0.61	
0.2	0.66	0.68	0.69	1.86	2.16	2.38	3.13	3.18	3.22	5.52			
0.3	0.14	0.30	0.46	0.5	0.51	0.56	0.61	0.80	0.84	1.06	1.82	3.25	
0.3	3.44	4.15											
0.4	0.59	0.88	1.10	1.74	2.14	2.67	3.31	4.33	4.39	4.53	5.52		
0.5	0.25	0.58	0.73	1.02	1.09	1.16	1.70	2.01	2.22	2.33	3.33	4.62	

Upon placing the drop onto the substrate immersed in the acidic aqueous solution, the drop was transparent and consistent. However, over time, the drop experienced a gradual reduction in size. In the experiments, the parameters were the initial volume of the drop V_0 and the formic acid concentration c_a , as listed in Table 1. V_0 was varied from 0.1 to 5.5 mm³ and the acid concentration in the aqueous solution c_a was varied from 0.2 to 0.5 wt%.

The size view of the drop was monitored by using a contact angle meter (Kruss DSA100E, Germany). An upright microscope (Nikon Y-QT, Japan) equipped with a camera (Nikon DS-Fi3, Japan) was employed for top view observation. An image segmentation program was applied in image processing to extract the base diameter, radius, and contact angle of the drop.

Confocal Microscopic Imaging and Particle Image Velocimetry: A confocal microscope system (Leica DMi8, Germany) was used to capture the images of microdroplets within the host drop during dissolution. A hydrophilic glass substrate was used for a clear bottom view of the microdroplets. The host drop was labeled by Neil red (sublimed grade, ≥99.5%; Sigma-Aldrich), and the external aqueous solution was labeled by fluorescein 5(6)-isothiocyanate (high-performance liquid chromatography; Sigma-Aldrich) in green. Laser excitation with wavelengths of 532 and 685 nm were applied to activate the two dyes, respectively. An optical camera (Hamamatsu C13440, Japan) equipped with a 10× objective was used for the fluorescent imaging.

For particle image velocimetry (PIV) measurements, fumed silica particles (Aldrich Chemistry, 10–50 μm in the diameter) were added in the external solution. The contact angle meter was employed to record the particle motion around the drop at a frame rate of 10 Hz. The PIVlab toolbox in MATLAB was used to process the images to get the flow field. In the image processing, square interrogation windows of 32 pixels × 32 pixels corresponding to 220 μm × 220 μm with an overlap of 50% were used to obtain the velocity vectors.

Supporting Information

Supporting Information is available from the Wiley Online Library or from the author.

Acknowledgements

The authors thank Romain Billet, Kangkana Kalita, and Kai Leong Chong for the valuable discussions. D.L. acknowledges funding by the ERC Advanced Grant No. 740479-DDD and from the NWO MCEC project. B.X. is grateful for the support from the Engineering and Physical Sciences Research Council (EPSRC, UK) grant-EP/N007921. X.H.Z. acknowledges the funding support from the Natural Science and Engineering Research Council of Canada (NSERC)-Discovery Project, NSERC Alliance—Alberta Innovates Advance grants, the Canada Research Chair Program and Canada Foundation for Innovation, John R. Evans Leaders Fund.

Conflict of Interest

The authors declare no conflict of interest.

Data Availability Statement

The data that support the findings of this study are available in the supplementary material of this article.

Keywords

drop detachment, on-drop reaction, phase separation, stick-jump dissolution

Received: April 14, 2023

Revised: August 22, 2023

Published online:

- [1] Y. Lu, S. Sathasivam, J. Song, C. R. Crick, C. J. Carmalt, I. P. Parkin, *Science* **2015**, *347*, 1132.
- [2] N. Miljkovic, E. N. Wang, *MRS Bull.* **2013**, *38*, 397.
- [3] W. Xu, H. Zheng, Y. Liu, X. Zhou, C. Zhang, Y. Song, X. Deng, M. Leung, Z. Yang, R. X. Xu, Z. L. Wang, X. C. Zeng, Z. Wang, *Nature* **2020**, *578*, 392.
- [4] Z. Ma, J. Ai, Y. Shi, K. Wang, B. Su, *Adv. Mater.* **2020**, *32*, 2006839.
- [5] M. J. Kreder, J. Alvarenga, P. Kim, J. Aizenberg, *Nat. Rev. Mater.* **2016**, *1*, 15003.
- [6] L. Feng, S. Li, Y. Li, H. Li, L. Zhang, J. Zhai, Y. Song, B. Liu, L. Jiang, D. Zhu, *Adv. Mater.* **2002**, *14*, 1857.
- [7] Y. Zheng, X. Gao, L. Jiang, *Soft Matter* **2007**, *3*, 178.
- [8] Q. Sun, D. Wang, Y. Li, J. Zhang, S. Ye, J. Cui, L. Chen, Z. Wang, H.-J. Butt, D. Vollmer, X. Deng, *Nat. Mater.* **2019**, *18*, 936.
- [9] P. Papadopoulos, L. Mammen, X. Deng, D. Vollmer, H.-J. Butt, *Proc. Natl. Acad. Sci. U. S. A.* **2013**, *110*, 3254.
- [10] J. B. Boreyko, C.-H. Chen, *Phys. Rev. Lett.* **2009**, *103*, 184501.
- [11] J. D. Smith, R. Dhiman, S. Anand, E. Reza-Garduno, R. E. Cohen, G. H. McKinley, K. K. Varanasi, *Soft Matter* **2013**, *9*, 1772.
- [12] F. Schellenberger, J. Xie, N. Encinas, A. Hardy, M. Klapper, P. Papadopoulos, H.-J. Butt, D. Vollmer, *Soft Matter* **2015**, *11*, 7617.
- [13] D. Daniel, J. V. I. Timonen, R. Li, S. J. Velling, J. Aizenberg, *Nat. Phys.* **2017**, *13*, 1020.
- [14] L. Chen, S. Huang, R. H. A. Ras, X. Tian, *Nat. Rev. Chem.* **2023**, *7*, 123.
- [15] Z. Wang, D. Orejon, Y. Takata, K. Sefiane, *Phys. Rep.* **2022**, *960*, 1.
- [16] H. Tan, C. Diddens, P. Lv, J. G. M. Kuerten, X. Zhang, D. Lohse, *Proc. Natl. Acad. Sci. U. S. A.* **2016**, *113*, 8642.
- [17] L. T. Raju, O. Koshkina, H. Tan, A. Riedinger, K. Landfester, D. Lohse, X. Zhang, *ACS Nano* **2021**, *15*, 4256.
- [18] C. C. Maass, C. Krüger, S. Herminghaus, C. Bahr, *Annu. Rev. Condens. Matter Phys.* **2016**, *7*, 171.
- [19] S. Michelin, *Annu. Rev. Fluid Mech.* **2023**, *55*, 77.
- [20] H. Tan, A. Banerjee, N. Shi, X. Tang, A. Abdel-Fattah, T. M. Squires, *Sci. Adv.* **2021**, *7*, eabh0638.
- [21] X. Wang, G. Liu, K. Wang, G. Luo, *Microfluid. Nanofluid.* **2015**, *19*, 757.
- [22] T. Ward, M. Faivre, H. A. Stone, *Langmuir* **2010**, *26*, 9233.
- [23] H. C. Mayer, R. Krechetnikov, *J. Appl. Phys.* **2013**, *113*, 174907.
- [24] M. Schmitt, H. Stark, *Phys. Fluids* **2016**, *28*, 012106.
- [25] D. Lohse, X. Zhang, *Nat. Rev. Phys.* **2020**, *2*, 426.
- [26] I. Lagzi, S. Soh, P. J. Wesson, K. P. Browne, B. A. Grzybowski, *J. Am. Chem. Soc.* **2010**, *132*, 1198.
- [27] C. Jin, C. Krüger, C. C. Maass, *Proc. Natl. Acad. Sci. U. S. A.* **2017**, *114*, 5089.
- [28] Z. Izri, M. N. van der Linden, S. Michelin, O. Dauchot, *Phys. Rev. Lett.* **2014**, *113*, 248302.
- [29] Z. Lu, M. H. K. Schaarsberg, X. Zhu, L. Y. Yeo, D. Lohse, X. Zhang, *Proc. Natl. Acad. Sci. U. S. A.* **2017**, *114*, 10332.
- [30] X. Zhang, J. B. You, G. F. Arends, J. Qian, Y. Chen, D. Lohse, J. M. Shaw, *Soft Matter* **2021**, *17*, 5362.
- [31] X. Yan, R. M. Bain, R. G. Cooks, *Angew. Chem., Int. Ed.* **2016**, *55*, 12960.
- [32] A. Fallah-Araghi, K. Meguellati, J.-C. Baret, A. El Harrak, T. Mangeat, M. Karplus, S. Ladame, C. M. Marques, A. D. Griffiths, *Phys. Rev. Lett.* **2014**, *112*, 028301.
- [33] D. Debuisson, A. Merlen, V. Senez, S. Arscott, *Langmuir* **2016**, *32*, 2679.
- [34] E. V. Ermayuk, N. V. Gavrilov, *J. Appl. Mech. Tech. Phys.* **2005**, *46*, 489.

- [35] R. Picknett, R. Bexon, *J. Colloid Interface Sci.* **1977**, *61*, 336.
- [36] M. Sokuler, G. K. Auernhammer, C. J. Liu, E. Bonaccorso, H.-J. Butt, *Europhys. Lett.* **2010**, *89*, 36004.
- [37] Y. O. Popov, *Phys. Rev. E* **2005**, *71*, 036313.
- [38] R. Billet, B. Zeng, J. Lockhart, M. Gattrell, H. Zhao, X. Zhang, *Soft Matter* **2022**, *19*, 295.
- [39] B. Romain, B. Zeng, H. Wu, L. James, G. Mike, H. Zhao, X. Zhang, *Droplet* **2023**, <https://doi.org/10.1002/dro2.82>.
- [40] E. Dietrich, S. Wildeman, C. W. Visser, K. Hofhuis, E. S. Kooij, H. J. W. Zandvliet, D. Lohse, *J. Fluid Mech.* **2016**, *794*, 45.
- [41] P. G. Jessop, L. Phan, A. Carrier, S. Robinson, C. J. Duerr, J. R. Harjani, *Green Chem.* **2010**, *12*, 809.